Development of a heat transport model for open-cell metal foams with high cell densities

Pedram Aghaei, Carlo Giorgio Visconti, Gianpiero Groppi, Enrico Tronconi *

Dipartimento di Energia, Laboratorio di Catalisi e Processi Catalitici, Politecnico di Milano, Via La Masa 34, I-20156 Milano, Italy

If made of highly conductive materials, open-cell metal foams are particularly interesting as enhanced catalyst supports for fast exo/endo-thermic reactions due to their excellent heat transfer properties. We have extended previous investigations by running heat transfer experiments on open-cell metal foams with very high porosity ($0.93 < e < 0.98$) and cell densities (60 and 110 PPI). The foam metal (FeCrAl alloy, NiCrAl alloy, copper, and cobalt), the temperature (300 □C–500 □C), the gas flow rate, and the flowing gas (N_2 and He) were varied. Heat transfer data were collected during steady-state heating runs by measuring temperatures at 22 axial positions and 3 radial positions in the cylindrically shaped foams. A classical 2D heat transfer model was developed based on various correlations available in the literature to describe the heat transport phenomena. Altogether, 20 parameters were optimized in this model: thermal conduction efficiencies and effective wall gap sizes for each of the 8 foams, 2 effective wall heat transfer parameters in the upstream zone for the two gases used, 1 parameter in the radiative contribution, and 1 parameter in the dispersive contribution. The optimized model obtained by global regression shows a very satisfactory fit of the data for all the foams at all the test conditions. Thermal conduction through the solid connected structure was found to play a major role in the effective radial conductivity, with a heat conduction efficiency mostly quite close to the often-used Lemlich value of 1/3. Static gas conduction through an effective gap at the foam-wall interface was identified as the dom-inant resistance in the wall heat transfer.

Highlights:
Open-cell metal foams promising catalyst supports due to high thermal conductivity.
Heat conduction efficiency was not far from the often-used Lemlich value of 1/3.
Heat transfer resistance at the wall increases with increasing foam cell diameter.
Structured tubular reactor wall heat transfer coefficient independent of flow rate.
Shorter reactors: process intensification, smaller pressure drop: cost efficiencies.

1. Introduction

Open-cell foams manufactured from different metals are interesting materials for a variety of applications due to their high surface area, mechanical strength, low relative density, and complex interfacial geometry. Their structure with highly interconnected porosity makes them good candidates for applications as heat exchangers, fuel cell electrodes, high-temperature filters, electron emitters, and catalyst supports [1–7]. In open-cell metal foams the cells are interconnected, with the frame structure consisting of pores communicating through windows [8–11]. As in other structured catalysts, the high porosity and the high surface/volume ratio result in a much lower pressure drop and a greater contact surface area between catalyst and reactants in a reactor filled with catalyzed foams rather than with packed particles [6–16]. Also, open-cell metal foams as catalyst supports offer the advantage of radial mixing within their structure and enhanced mass transfer because of the tortuosity of flow in comparison to segregated laminar flow in honeycomb monoliths with no lateral mixing between channels [6–16]. The poor effective thermal conductivity of conventional packed-bed catalysts for highly exothermic and

---

* Corresponding author.
    E-mail address: enrico.tronconi@polimi.it (E. Tronconi).

endothermic heterogeneous reactions may result in catalyst deactivation and a decrease in productivity and/or product selectivity [14–16]. In comparison to conventional packed-bed catalysts, thermally connected structured catalyst supports made of highly conductive metals can improve the heat transfer efficiency [14–16]. Moreover, open-cell metal foams as catalyst supports can be manufactured in different geometries allowing for the adjustment of axial or radial flow patterns in the structured reactor [11–15]. From an industrial point of view, the structured catalysts are beneficial since they have the advantages of (i) enabling manufacture of smaller reactors, (ii) providing higher yields and selectivities particularly in heat and mass transfer limited processes, and (iii) improving temperature control, heat management and safety in non adiabatic reactors [14–26].

Despite the great interest in the potential of these new materials as catalyst supports, there is still a lack of engineering models available in the open literature for the estimation of effective heat transfer coefficients in reactors loaded with metal foam catalysts at temperatures and flow rate conditions relevant for chemical processes.

For open-cell metal foams saturated with a medium, many experimental data and theoretical heat transfer models have been reported in the open literature considering explicitly the dominating stagnant (conduction) contribution and neglecting thermal radiation and convection [7,27–43]. These works can be classified as: (i) asymptotic solutions, proposing theoretical correlations originally derived for the estimation of the electric conductivity; however, by analogy these correlations can also be used for the prediction of the thermal conductivity [28–35]; (ii) unit cell approaches, suggesting theoretical models based on simplified descriptions of the foam cell considering the cell distribution homogenous/periodic in the structure, hence, e.g. the overall conductivity of the foam is represented by that of a single unit cell [27,36–42], and (iii) empirical correlations fitted to experimental data without making any assumption on the shape of the single cell; nonetheless relying on experimental data collected on a single foam sample [7,27,35,43].

In previous works, some of us reported heat transfer measurements over open-cell FeCrAl alloy and aluminum (Al–6101) foams with different cell diameters ranging from 1.55 mm to 5.09 mm [44,45]. The data pointed out the benefits of adopting foams with small cell diameters, which enhance the wall heat transfer in addition to increasing the interfacial area. In this work the investigation has been extended to eight new FeCrAl alloy, NiCrAl alloy, cobalt, and copper open-cell metal foams with cell diameters ranging from 0.58 to 1.2 mm, i.e. much smaller than those previously investigated [44,45]. The experimental results have been analyzed by global regression to develop and fit a general model of heat transfer in foams, which can be used to predict the heat transfer behavior of comparable foam materials.

2. Materials and methods

2.1. Investigated foam samples

The samples investigated in this work were open-cell metal foams made of FeCrAl alloy (foams A, B), NiCrAl alloy (foams C, D), cobalt (foams E, F), and copper (foams G, H), all supplied by Alantum Europe GmbH [46].

The thermal conductivities of the fabrication material of the foams, k_s [W m^{-1} K^{-1}], were obtained from data in the open literature. For the FeCrAl alloy material, based on the composition of the alloy (Fe:Cr:Al = 73:21:6), the solid conductivity can be expressed as a linear function of temperature [44,47]:

$$k_s = 11.103 + 0.014T; \quad 270K < T < 1200K \tag{1}$$

For the NiCrAl alloy foam, the solid conductivity as a function of the temperature was obtained from heat transfer handbooks [48,49]. Excel software was used to find the optimal polynomial equation through these data:

$$k_s = 9.29 + 9.95 \times 10^{-3}T + 5.71 \times 10^{-6}T^2; \quad 523K < T < 873K \tag{2}$$

For copper and cobalt foams the following expressions were used [48,49]:

$$\text{Cobalt} : k_s = 97.2 - 0.04909T; \quad 523K < T < 823K \tag{3}$$

$$\text{Copper} : k_s = 402.3 - 0.0567T; \quad 523K < T < 823K \tag{4}$$

The solid densities of the applied materials were taken from the open literature: 7.65 g cm^{-3} for FeCrAl alloy, 8.4 g cm^{-3} for NiCrAl alloy, 8.9 g cm^{-3} for cobalt, and 8.96 g cm^{-3} for copper.

2.2. Fluid thermal properties

For the flowing gases, nitrogen and helium, gas properties such as thermal conductivity, k_f [W m^{-1} K^{-1}], heat capacity, $C_{p,G}$ [J kg^{-1}], and gas viscosity, μ_G [kg m^{-1} s^{-1}] have been reported in Table 1 as temperature-dependent relationships and applied in stagnant and dispersive contributions to the radial effective thermal conductivity (k_{er}) [50].

2.3. Morphological characterization

2.3.1. Gravimetric analysis

The open-void fraction in a cellular solid is defined as the ratio between the void volume and the total volume [44,45]. Optical microscopy in this and in previous works [44,45] showed that the struts of some foams are hollow, not solid, see Fig. 1.

Therefore, two different porosities are defined for the open-cell metal foams: total porosity and hydrodynamic porosity. The hydrodynamic porosity, or open-void fraction, is the total porosity minus the void volume in the hollow struts [6,44,51], since this void volume is hardly accessible, neither for the reactants nor for the catalytic washcoat. The total porosity, ε_T, thus includes all void space, while the hydrodynamic porosity, ε_H, includes only the accessible void space [6,44,51]. The open-void fraction in terms of densities was determined as follows [6,44,51,52]:

$$\varepsilon_H = 1 - \frac{\rho_{foam}}{\rho_{HS}}, \tag{5}$$

$$\varepsilon_T = 1 - \frac{\rho_{foam}}{\rho_{solid}} \tag{6}$$

where, ε_T: total porosity [–]; ε_H: hydrodynamic porosity [–]; ρ_{foam}: foam mass density [kg m^{-3}]; ρ_{solid}: mass density of bulk material [kg m^{-3}]; ρ_{HS}: mass density of hollow struts [kg m^{-3}].

The foam density, ρ_{Foam}, is estimated by dividing the weight of the foam by its total measured volume, based on the cylindrical shape of the foam sample:

$$\rho_{foam} = \frac{W_{foam\ in\ air}}{V_{foam}} = \frac{W_{foam\ in\ air}}{\pi(D_{foam}/2)^2 L_{foam}} \tag{7}$$

where, $W_{foam\ in\ air}$: weight of foam in air [kg]; V_{foam}: volume of foam (in this study and previous studies [44,45] cylindrical shape) [m^3]; D_{foam}: foam diameter [m]; L_{foam}: foam length [m].

The density of the hollow struts, ρ_{HS}, is determined by using a standard pycnometry method; based on the experimental measurements of the buoyancy of the foam samples in ethanol this can be expressed as [6,44,51]:

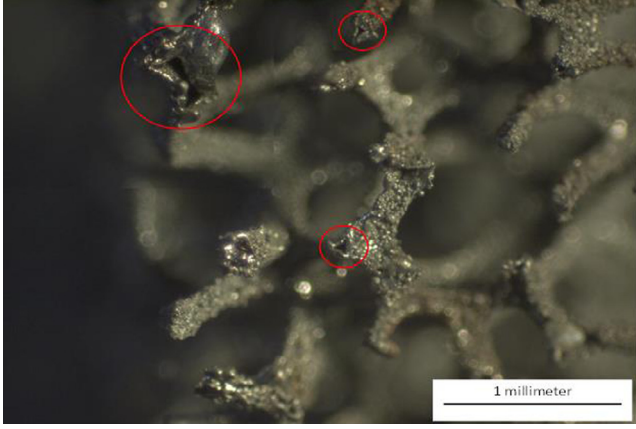|	Nitrogen (N_2)	Helium (He)
$C_{p,G}$ [J kg^{-1}]	$1103.2 - 0.4428T + 9.0 \times 10^{-4}T^2 - 4.0 \times 10^{-7}T^3$	5193
μ_G [kg m^{-1} s^{-1}]	$10^{-6}(30.43 + 0.4989T - 1.1 \times 10^{-4}T^2$	$10^{-6} \times (54.16 + 0.5014T - 8.947 \times 10^{-5}T^2$
k_f [W m^{-1} K^{-1}]	$4.18 \times 10^{-4}(0.936 + 0.234T - 1.21 \times 10^{-4} \times T^2 + 3.59 \times 10^{-8}T^3$	$4.18 \times 10^{-4}(88.89 + 0.93T - 1.79 \times 10^{-4}T^2 + 3.09 \times 10^{-8}T^3$

Fig. 1. Typical hollow struts of open-cell metal foam samples. FeCrAl alloy foam sample, foam A supplied by Alantum Europe GmbH [46]. (Magnification of 40×).

$$\rho_{HS} = \frac{W_{foam\ in\ air}\,\rho_{ethanol}}{W_{foam\ in\ air} - W_{foam\ in\ ethanol}} \qquad (8)$$

where, $\rho_{ethanol}$: pure ethanol density at room temperature [kg m^{-3}].

Pure ethanol is used for the measurements since water is unable to access the entire void volume inside the foams, therefore, leaving air bubbles attached to the structure due to poor wetting and surface tension effects [6,44,51,52]. The hydrodynamic porosity is the relevant parameter for investigations regarding mass transfer and pressure drop of foams used as catalyst supports, while the total porosity must be taken into account in the evaluation of the effective heat conductivity [6,44,51,52].

2.3.2. Optical microscope analysis

The structure of open-cell metal foams consists of solid interconnected struts that enclose a cell, Fig. 2(b). Pores in the cell are determined as the openings (windows) of the cell, Fig. 2(a). Micrographs were taken with an optical microscope (Olympus SZ-CTV 40) for each sample, as shown in Fig. 3, to characterize and mea-sure the foam samples by measuring their pore, cell, and strut diameters in the middle, d_p [m], d_c [m], and t_s [m], respectively. The elliptical (oval) shapes of the cell and pore consist of two diameters, short and long diameters, as indicated in Fig. 2(a). For each foam sample, several measurements were taken and the average of the short and long diameters was chosen for the cell and pore diameters for that foam.

The strut cross section of the metal foams is not constant but becomes larger moving from the center of the filament (where the strut diameter is measured) towards the intersections with other struts. This has a substantial influence on heat conduction in the metal foam since at fixed porosity the concentration of the metal solid at the ends of the ligaments results in decreasing the heat conduction and therefore in a lower conduction efficiency due to the limitation associated with the thinnest strut section [44,53,54].

The average values of the geometrical properties (d_c, d_p, t_s) of the investigated open-cell metal foams are reported in Table 2 together with standard deviations. Large relative standard deviations were observed for d_p (>40%). On the other hand, relative deviations <20% were observed for d_c. Note that the nominal values of d_c provided by the manufacturer are within the experimental uncertainty of the measurements, accordingly such nominal values have been used in the correlations described in this work.

Since the open-cell metal foams provided by Alantum Europe GmbH [46] had a disc shape with diameter of 28 mm and thicknesses of 1.7–3 mm, up to 60 foam discs had to be stacked on top of each other to obtain a 100 mm cylindrical foam sample for the heat transfer runs (see below).

3. Heat transfer measurements

3.1. Experimental rig

The heat transfer measurements were carried out in a dedicated test rig. This heat transfer rig includes a stainless steel (AISI 316) tubular reactor inserted into a thermostatic oven with air recirculation and loaded with the foam samples, Fig. 4. The tested foam
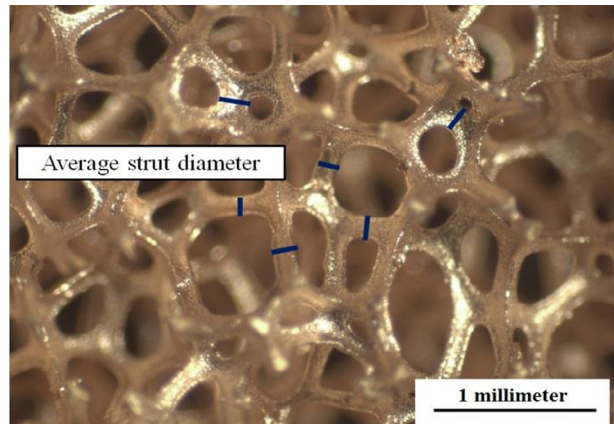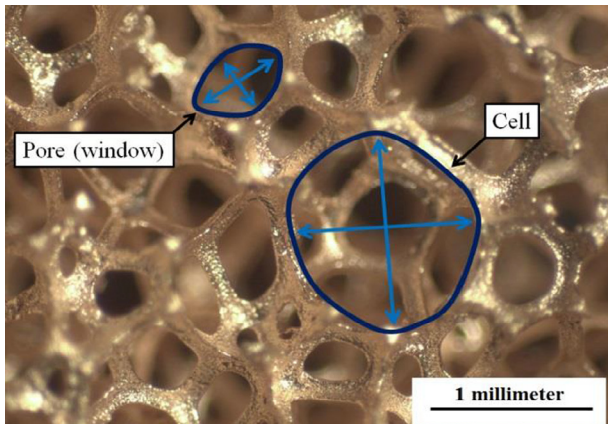

Fig. 2. (a) Description of cell and pore and approach for measuring the cell and pore diameters in open-cell metal foams (b) middle section in the strut measured for the average strut diameter, t_s.
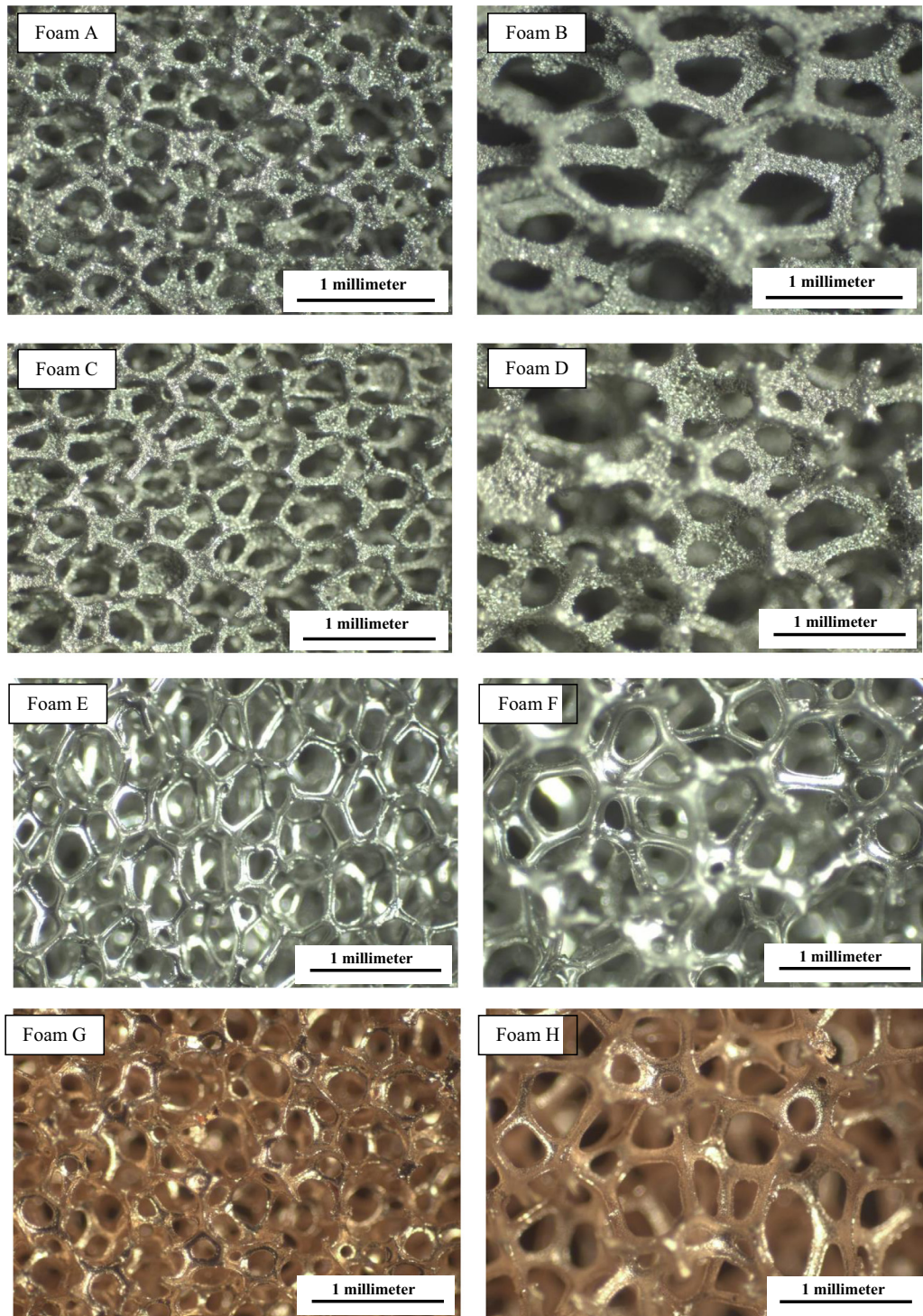
Fig. 3. Optical micrographs of all the 8 investigated open-cell metal foams with magnification of 40×. Foam A: FeCrAl alloy d_c = 0.58 mm, Foam B: FeCrAl alloy d_c = 1.2 mm, foam C: NiCrAl alloy d_c = 0.58 mm, Foam D: NiCrAl alloy d_c = 1.2 mm, foam E: cobalt d_c = 0.58 mm, Foam F: cobalt d_c = 1.2 mm, Foam G: copper d_c = 0.58 mm, Foam H: copper d_c = 1.2 mm.

samples have a cylindrical shape with an external diameter of 28 mm (D_{foam}) and a length of 100 mm (L_{foam}). We tried to our best to push the foam discs together and avoid any space between them to shape up a 100 mm length and 28 mm diameter cylinder. The inner diameter of the stainless steel reactor tube was equal to the outer diameter of the foam sample, 28 mm, minimizing bypass at the wall. Since it is impossible to achieve a perfect fit due to minor deviations from the perfect cylindrical shape, however, a

small gap at the wall of typically 0.1 mm was unavoidable. All the foam samples had three axial through holes with a diameter of 3.28 mm at different radial positions, namely center (r = 0), half radius (r = 7 mm), and two-third radius (r = 9 mm). Note that the total volume of the three holes is only 4% of the foam volume, thus having a minor impact on the overall void and solid fractions. Three 1/8′ (3.18 mm) stainless steel thermowells were inserted inside these three through holes, tightly fitted in order to avoid

Table 2
Geometrical properties of the investigated metal foam samples.

| Foam	Material	ε_T	ε_H	d_c [mm] nominal	d_c [mm] measured	d_p [mm]	t_s [mm]
A	FeCrAl alloy	0.93	0.90	0.58	0.61 ± 0.09	0.19 ± 0.07	0.08 ± 0.01
B	FeCrAl alloy	0.95	0.94	1.20	1.31 ± 0.26	0.49 ± 0.20	0.18 ± 0.02
C	NiCrAl alloy	0.93	0.92	0.58	0.63 ± 0.11	0.23 ± 0.08	0.07 ± 0.01
D	NiCrAl alloy	0.95	0.95	1.20	1.11 ± 0.15	0.30 ± 0.10	0.14 ± 0.04
E	Cobalt	0.97	0.95	0.58	0.60 ± 0.08	0.26 ± 0.10	0.07 ± 0.01
F	Cobalt	0.98	0.97	1.20	1.10 ± 0.12	0.34 ± 0.10	0.12 ± 0.02
G	Copper	0.96	0.95	0.58	0.65 ± 0.11	0.21 ± 0.07	0.07 ± 0.02
H	Copper	0.97	0.96	1.20	1.11 ± 0.16	0.34 ± 0.14	0.13 ± 0.02
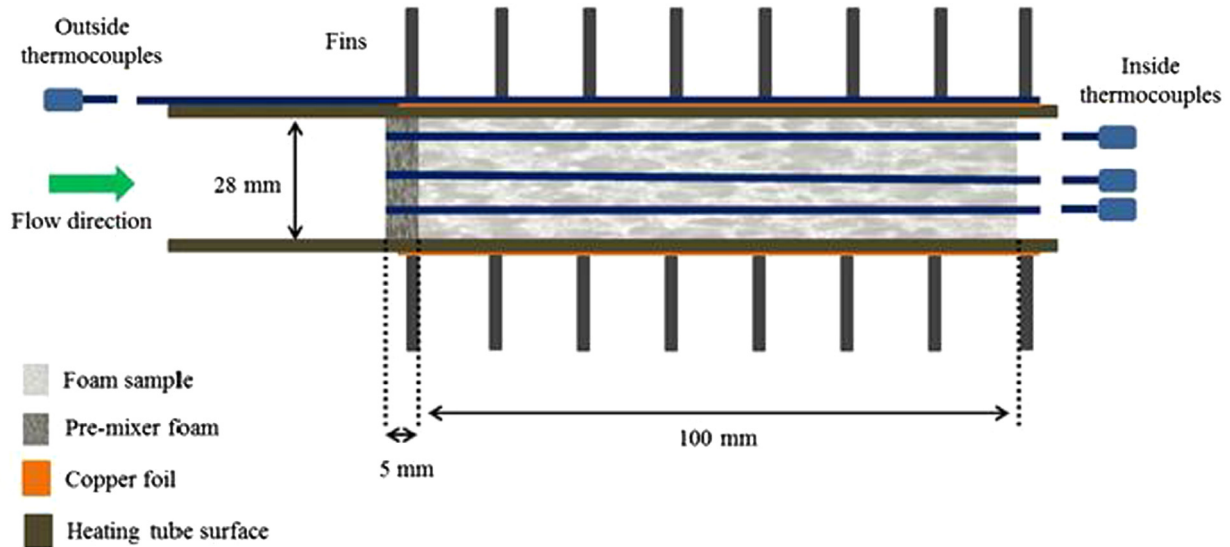
Fig. 4. Schematic representation of the test tube, loaded with foam sample, pre-mixer foam, 8 external fins, and 3 inside (center (r = 0), half radius (r = 7 mm), and two-third radius (r = 9 mm)) and 1 outside (reactor surface) thermowells.

local bypass phenomena, and equipped with sliding K-type thermocouples. The fourth thermocouple was tightly fitted to the external surface of the reactor tube, thus measuring the temperature of the tube external surface. These four thermocouples hence provided the temperature profiles in the foam (in 3 radial positions and 21 axial positions) and also in the reactor tube wall along the foam bed. In view of their very limited volume fraction, a significant effect of the holes (and of the thermowells) on the effective radial conductivity of the foam matrix is unlikely.

The reactor tube was equipped with eight external fins on the outer surface for a better external heat transfer. A thin layer of copper foil was rolled around the reactor before placing the external fins on it in order to ensure an optimal thermal contact between the reactor surface and the external fins. At the upstream zone, 5 mm before the foam sample, one additional cylindrical FeCrAl alloy foam (5 mm length and 28 mm outer diameter) was placed in tight contact with the foam sample to improve the uniformity of the radial gas velocity and temperature profiles.

3.2. Experimental methods

Two different flowing gases were chosen for the heat transfer experiments, i.e. nitrogen (N_2) and helium (He). Both gases were fed to the system at atmospheric pressure and regulated by a mass flow controller at room temperature. After the gases reached the reactor, they were pre-heated by the oven before introducing them to the metal foam. For each operating condition and foam sample tested, three different flow rates, 25, 30 and 35 Nl min^{-1} (GHSV $\cong$ 24000, 29000 and 34000 h^{-1}) and two different oven

set point temperatures, 300 °C and 500 °C, were used. After reaching steady-state conditions, temperature profiles were measured with a spatial resolution of 5 mm along the bed length, at the reactor tube outer wall, and inside the foams. The attainment of steady-state conditions was checked by measuring the axial temperature profile of the foam at least twice (by sliding the thermocouples) to assure that there was no changes in time.

Four typical examples of temperature profiles measured over the foam samples are presented in Fig. 5, showing the influence of the different gases on two different foam materials: a poorly and a well conducting foam (NiCrAl alloy, $k_s \approx 20$ W m^{-1}K^{-1} and copper with $k_s \approx 360$ W m^{-1}K^{-1}) at 500 °C and at 20 and 30 Nl min^{-1}. The transfer of heat from the reactor tube wall to the foam samples along the foam length is clearly visible in all the profiles. At the beginning of the foam bed (the upstream side) the radial temperature gradients between the reactor tube wall and the foam centerline are larger due to the colder gas flowing in at the entrance. Comparison of Fig. 5a with Fig. 5b shows the influence of the thermal conductivity of the gas. By comparing the results obtained at approximately the same specific heat flow (the heat capacity of N_2 is about 1.5 times larger than that of He, therefore we compare the results for 20 Nl min^{-1} N_2 with those for 30 Nl min^{-1} He), the radial temperature gradients, i.e. the temperature differences between center, 7 mm, and 9 mm, are significantly smaller in He than in N_2. This indicates that the overall heat transfer efficiency increases when using He gas. Additionally, comparison of the results for the NiCrAl alloy foam with those for copper foam shows that a high metal solid thermal conductivity flattens the radial temperature gradients in the foam. The higher
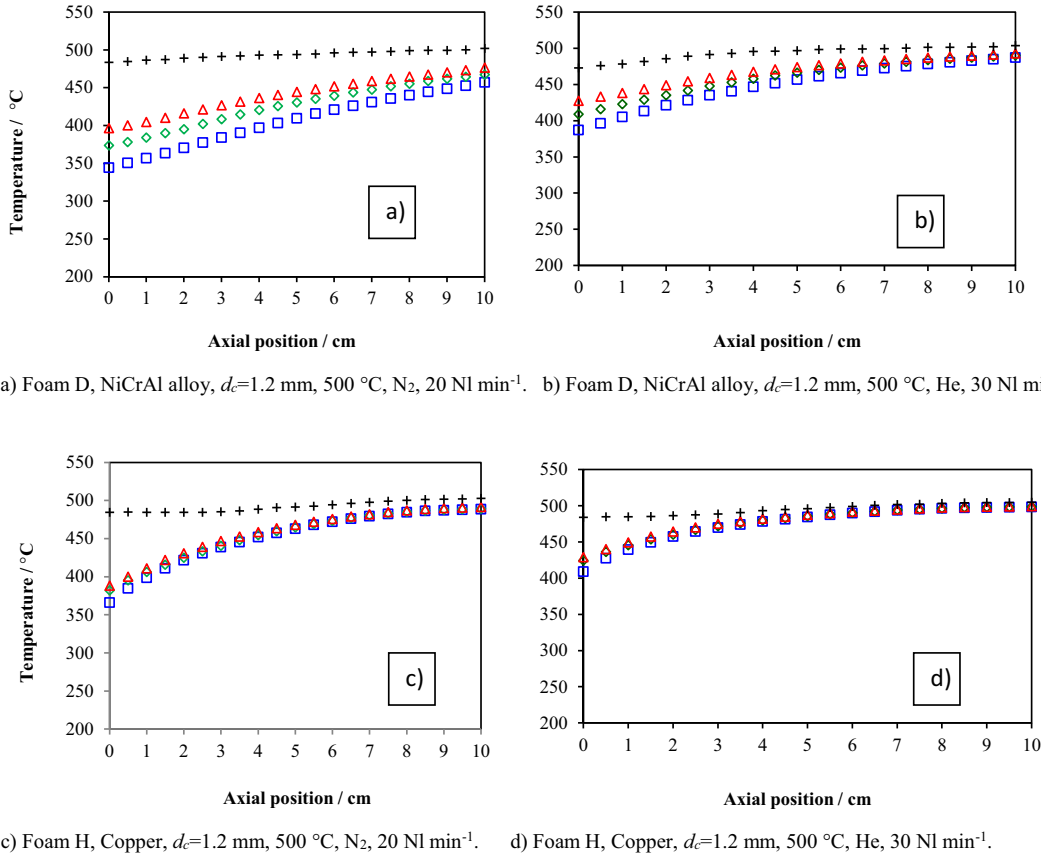
a) Foam D, NiCrAl alloy, d_c=1.2 mm, 500 °C, N$_2$, 20 Nl min^{-1}. b) Foam D, NiCrAl alloy, d_c=1.2 mm, 500 °C, He, 30 Nl min^{-1}.

c) Foam H, Copper, d_c=1.2 mm, 500 °C, N$_2$, 20 Nl min^{-1}. d) Foam H, Copper, d_c=1.2 mm, 500 °C, He, 30 Nl min^{-1}.

Fig. 5. Measured axial temperature profiles for the mentioned foam samples. Results are shown at four different radial positions in the tube: center, 1/2, 2/3 radius and reactor tube wall. These are indicated with Exp(0) □, Exp(1/2) ◊, Exp(2/3) △, and Wall +, respectively.

thermal conductivity of He and the higher solid thermal conductivity of copper, boosting up the heat transfer, yield the fastest approach of the foam centerline temperature to the wall temperature (Fig. 5d). When running an exothermic reaction over foams washcoated with a catalyst and loaded in a tubular reactor with external cooling, this configuration would yield the optimal heat management, as it would minimize the formation of hot spots which typically cause selectivity losses, risks of unstable operation and catalyst deactivation.

3.3. Two-dimensional heat transfer model

A two-dimensional, pseudo-homogenous, steady-state heat transfer model has been developed to estimate the heat transfer parameters by nonlinear regression of the experimental data. It is assumed that the heat transfer between the flowing gas and the metal foam is fast enough to guarantee a negligible temperature difference between the gas and the solid phases. Such an approximation is well matched for the high pore density foams herein investigated in view of their very high specific geometric areas, which are estimated to be about 2000 m^{-1} and 3500 m^{-1}, based on the geometrical parameters reported in Table 2 for samples with cell diameters of 1.2 mm and 0.58 mm respectively [55].

Accordingly, the differential energy balance in the foam is expressed in cylindrical coordinates as:

$$W_{in}c_p\frac{\partial T}{\partial x} = k_{er}\left(\frac{1}{r}\frac{\partial T}{\partial r} + \frac{\partial^2 T}{\partial r^2}\right) + k_{ea}\left(\frac{\partial^2 T}{\partial x^2}\right) \tag{9}$$

where, W_{in}: specific mass velocity [kg s^{-1} m^{-2}]; C_p: specific heat capacity [kJ kg^{-1} K^{-1}]; T: temperature [K]; r: radial coordinate [m]; x: axial coordinate [m]; k_{er}: radial effective conductivity [W m^{-1} K^{-1}]; k_{ea}: axial effective conductivity [W m^{-1} K^{-1}].

The above second-order partial differential equation (PDE) is derived assuming the absence of chemical reactions inside the foam. Moreover, it is assumed that the heat generation due to the friction of the flowing gas through the porous foam is negligible, thus neglecting viscous dissipation and pressure work. The temperature increase due to frictional heat generation is indeed negligibly small due to the small pressure drop and the large heat input into the foam from the reactor tube wall.

Additionally, the terms accounting for the dependency of the effective conductivities on the temperature, and consequently the radial and axial position have been neglected. In order to validate this simplification the actual values of the term accounting for the dependency of the effective conductivity in radial direction, i.e. $(\partial k_{er}/\partial T)(\partial T/\partial r)$ were calculated and found to be mostly less than 3% and at maximum 8% of the value of sum of the other terms on the right hand side of Eq. (9). For the term accounting for the dependency of the effective conductivity in axial direction, i.e. $(\partial k_{ea}/\partial T)(\partial T/\partial x)$ the influence was even much smaller due to the small influence of axial conduction.

Two boundary conditions in both radial and axial directions are needed for Eq. (9). For the radial direction, a symmetry boundary condition at the centerline is assumed. This means that at the centerline there is no temperature gradient:

$$\frac{\partial T}{\partial r} = 0, \quad at : r = 0 \tag{10}$$

A second boundary condition for the radial direction derives from the steady-state condition at the edge of the metal foam; it is assumed that the heat flux leaving the foam outer surface, k_{er} $(\partial T/\partial r)$, is equal to the heat transfer from the foam outer surface to the reactor tube wall, h_w $(T_{x,w} - T_{x,r=R})$:

$$k_{er}\frac{\partial T}{\partial r} = h_w (T_{x,w} - T_{x,r=R}), \quad at : r = R \tag{11}$$

where, h_w: wall heat transfer coefficient [W m^{-2} K^{-1}]; $T_{x,w}$: reactor tube surface temperature at axial coordinate x [K]; $T_{x,r=R}$: foam surface temperature at axial coordinate x [K].

For the axial direction, an adiabatic condition is assumed at the end of the foam. This implies no temperature gradient at the foam outlet. Moreover, a Danckwerts type boundary condition is applied at the foam entrance [56,57], where it is assumed that the diffusive heat flux equals the convective heat transport into the foam.

$$\begin{cases} k_{ea}\frac{\partial T}{\partial x} = W_{in}C_p (T_{x=0,r} - T_{x=-\infty,r}), & at : x = 0 \\ \frac{\partial T}{\partial x} = 0, & at : x = L \end{cases} \tag{12}$$

The upstream temperature ($T_{x=-\infty,r}$) in the boundary condition at x = 0 in Eq. (12) was evaluated from measurements taken 5 mm upstream from the foam inlet (x = −5 mm).

The method adopted for estimating the radial temperature profile applied for the inlet boundary condition is described in Appendix A.

The PDE model is solved numerically applying the finite differences method with 2000 discretization points in the axial direction, using the upwind first-order scheme, and the orthogonal collocation method with 8 collocation points [58] in the radial direction.

The three adaptive parameters in this model are the radial effective conductivity (k_{er}), the axial effective conductivity (k_{ea}), and the wall heat transfer coefficient (h_w). These three parameters contain heat transport contributions by conduction, dispersion (convection), and radiation, which are dependent on foam properties, flow rates, gas type, and temperature, and which are included via correlations involving the parameters to be optimized, as discussed later. A non-linear regression, based on minimization of the sum of squared differences between experimental and calculated temperature data, is used to obtain the optimal estimates of these parameters. The least-squares regression was carried out using the software package Athena Visual Studio [59], which relies on a combination of estimation algorithms, including the Levenberg-Marquardt method.

4. Heat transfer correlations derived from global regression

4.1. Estimation of the radial and axial effective conductivity (k_{er} and k_{ea})

The heat transfer mechanisms which can contribute to the overall heat transport include: (i) heat transfer by conduction via the struts of the metal foams, (ii) dispersive heat transfer due to mechanical dispersion of the fluid flowing through the foam porous structure, and (iii) radiative heat transfer, which could become particularly significant at higher temperatures [48,49].

From the three contributions mentioned above, it is possible to formulate the effective radial conductivity as the sum of these contributions by conduction (k_{stag}), dispersion (k_d), and radiation (k_{rad}) [44]:

$$k_{er} = k_{stag} + k_d + k_{rad} \tag{13}$$

where, k_{er}: radial effective conductivity [W m^{-1} K^{-1}]; k_{ea}: axial effective conductivity [W m^{-1} K^{-1}] k_{stag}: total radial effective stagnant thermal conductivity [W m^{-1} K^{-1}]; k_d: isotropic dispersive

thermal conductivity [W m^{-1} K^{-1}]; k_{rad}: radiative thermal conductivity [W m^{-1} K^{-1}].

4.2. Stagnant radial thermal conductivity

Empirical correlations have been proposed by several authors to fit their experimental heat transfer data. A preliminary analysis suggests that the empirical correlation presented by Calmidi et al. [27] is well able to describe the heat conduction through the solid and fluid phases in the metal foams used in this study. Their correlation is based on a model in which the heat conduction through the solid and the fluid phases occurs in parallel; as a consequence, the overall stagnant thermal conductivity is the sum of the contributions of both phases [27]:

$$\frac{k_{stag}}{kf} = \varepsilon_T + A(1 - \varepsilon_T)^n \frac{k_s}{k_f} \tag{14}$$

where, k_{stag}: total radial effective stagnant thermal conductivity [W m^{-1} K^{-1}]; k: thermal conductivity [W m^{-1} K^{-1}]; f and s: refer to fluid and solid, respectively; ε_T: total porosity [–]; A : conduction efficiency [–]; n: fitting constant [–].

The authors obtained the best fit with n = 0.763 and A = 0.181 for air and 0.195 for water [27]. In our work, it was not possible to estimate A and n independently since we do not have foams of the same material and same structure with significantly different porosities. Therefore, it was decided to fix n at the value of 1 to enable a direct comparison of the fitted values of A with the value of 1/3 in the also frequently used simpler Lemlich model [30]:

$$k_{stag} = \frac{1}{3}(1 - \varepsilon_T)k_s \tag{15}$$

In this respect, the gas contribution to the stagnant conductivity was neglected. The optimized values of the A parameters for all the tested foams, under the assumption of equal axial and radial effective conductivity (which is discussed hereafter), lie in a rather narrow range between 0.26 and 0.38 as shown in Table 3, which is around the Lemlich value of 1/3. This narrow range suggests that the A parameters of all open-cell metal foams with a comparable structure are probably close to the often used Lemlich value.

The influence of the effective axial conductivity (k_{ea}) on the fit results was found to be very small compared to the effective radial conductivity (k_{er}), possibly due to the large aspect ratio of the foam samples (length/diameter = 100/28). To document this, the quality of the fit (i.e. the SSQ = sum of the squared residuals) is plotted at different fixed k_{ea}/k_{er} ratios in Fig. 6. The best fit was obtained with k_{ea}/k_{er} = 1, although the results at k_{ea}/k_{er} = 0.33, 0.5, and 0.75 are only slightly worse. k_{ea}/k_{er} is likely somewhat less than one in our experimental setup as a result of additional axial resistances due to the limited number of contact points between the foam discs (the discs are probably not in perfect contact). Nevertheless, Fig. 6 clearly shows that setting k_{ea}/k_{er} to zero, as done e.g by Wallenstein et al. [60], provides a poor fit of our data. Based on the above fit results, however, k_{ea}/k_{er} = 1 is assumed to be the optimal ratio and used for estimating the other heat transfer parameter.

4.3. Dispersive thermal conductivity

In previous work [44], it has been noted that the contribution of the dispersive conductivity is not negligible when the stagnant conductivity is low. Dispersive thermal conductivity as a hydrodynamic phenomenon is directly proportional to the local flow velocity at high Péclet number [61]. For the forced convection of air in highly porous aluminum foams, the following model has been proposed to describe the dispersive conductivity [61–63]:

$$k_d = k_f C_d Re_K Pr \tag{16}$$

Table 3
The estimates of the fitting parameters, conduction efficiency (A), and effective gap size (Eff. gap size) for all the foams used in the heat transfer experiments along with 95% confidence ranges (see Appendix B for a consideration on the correlation between the experimental data).

Foam	A	B	C	D
	FeCrAl alloy	FeCrAl alloy	NiCrAl alloy	NiCrAl alloy
A [-]	0.261 ± 0.003	0.291 ± 0.005	0.379 ± 0.004	0.328 ± 0.005
Eff. gap size [mm]	0.260 ± 0.008	0.436 ± 0.012	0.185 ± 0.007	0.169 ± 0.008
Foam	E	F	G	H
	Cobalt	Cobalt	Copper	Copper
A [-]	0.316 ± 0.004	0.302 ± 0.005	0.260 ± 0.006	0.258 ± 0.005
Eff. gap size [mm]	0.205 ± 0.005	0.310 ± 0.008	0.177 ± 0.002	0.251 ± 0.003

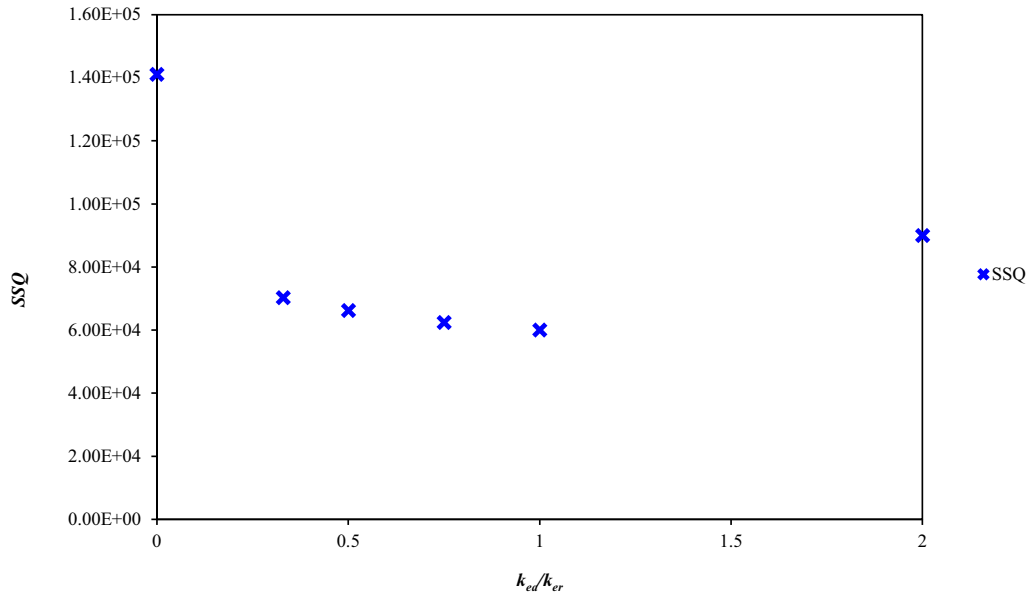N.B. See Appendix B for a more realistic estimate of the confidence ranges.

Fig. 6. The sum of the squared residuals (SSQ) for all the 8 tested foams versus the ratio of axial to radial effective conductivity (k_{ea}/k_{er}).

$$Re_K = \frac{\rho_G u_0 \sqrt{K_{per}}}{\mu_G} \quad (17)$$

$$Pr = \frac{\mu_G C_{p,G}}{k_f} \quad (18)$$

where k_d: dispersive thermal conductivity [W m^{-1} K^{-1}]; C_d: thermal dispersion coefficient [–]; Re_K: Reynolds number based on permeability [–]; Pr: Prandtl number [–]; ρ_G: gas density [kg m^{-3}], u_0: superficial gas velocity [m s^{-1}], K_{per}: permeability [m^2], μ_g: gas viscosity [kg s^{-1} m^{-1}], $C_{p,G}$: gas heat capacity [kJ kg^{-1} K^{-1}].

The Reynolds number Re_K is based on the square root of the permeability, K_{per} [m^2], for which Calmidi and coworkers [27,35] reported the following correlation, valid for open-cell metal foams:

$$K_{per} = 0.00073 \, d_P^2 (1 - \varepsilon_T)^{-0.224} \left(\frac{t_s}{d_P}\right)^{-1.11} \quad (19)$$

where d_p: average pore inner diameter [m], ε_T: total porosity, t_s: average strut thickness in the middle [m].

Calmidi and co-workers [64] obtained an estimate of $C_d = 0.06$ by fitting the data from Hunt and Tien [61] for polyurethane foams. In our investigation, C_d was fixed at this value since the sensitivity of our regression to the C_d value was too small to allow a reliable estimation, probably as a result of the small foam cell size, and consequently, a very small contribution of the dispersion term compared with the stagnant one associated with the high conductivity of metallic matrices.

4.4. Radiative thermal conductivity

The contribution by radiation to the radial effective thermal conductivity is expected to increase rapidly with temperature [47]. The effective radiative conductivity based on a modified diffusion approximation of the Rosseland equation is determined as [65]:

$$k_{rad} = \frac{16\sigma T^3}{3\beta} \quad (20)$$

where, σ: Stefan-Boltzman constant 5.67×10^{-8} [W m^{-2} K^{-4}]; T: temperature [K]; β: Rosseland extinction coefficient [m^{-1}].

The Rosseland extinction coefficient, β, is the sum of absorption and scattering coefficients and the inverse of the penetration thickness of radiation [47]. This coefficient can be experimentally estimated by spectrophotometric measurements, integrating the monochromatic extinction coefficient over the whole spectrum [65]. However, this approach is quite complex and therefore in the literature empirical relations were developed connecting the extinction coefficient with geometrical characteristics of foams such as pore size and porosity [62], while the influence of solid emissivity on the equivalent radiative conductivity was found to be negligible [63]. The following correlation was proposed to calcu-

late the Rosseland extinction coefficient as a function of the structural properties of metal foams [65]:

$$\beta = C_{Ross.} \frac{\sqrt{(1-\varepsilon_H)}}{d_c} \tag{21}$$

where, $C_{Ross.}$: geometrical fitting parameter [–]. For the geometrical fitting parameters different values $C_{Ross.}$ = 2.65 and $C_{Ross.}$ = 4.09 have been obtained based on the best fit in different works [65,66]. In our work, the optimal fit was obtained with $C_{Ross.}$ = 6.46 ± 0.37.

4.5. Wall heat transfer coefficient

The following correlation for the wall heat transfer coefficient h_w is used to consider the dependency of h_w on the static contribution at the wall, on the Reynolds and the Prandtl numbers of the flowing gasses, and on a radiative contribution [48,49]:

$$h_w = h_{Static} + h_{Convection} + h_{Radiation} \tag{22}$$

The static contribution, h_{static} [W m^{-2} K^{-1}], was calculated as:

$$h_w = h_{static} = k_f / Eff. \, gap \, size \tag{23}$$

This corresponds to the heat transfer resistance to heat conduction across a stagnant gas layer between two planes at a short distance. The distance between the two planes, i.e. the effective gap (Eff. gap size), was estimated for each foam separately, resulting in physically acceptable values in the range 0.17–0.44 mm, as represented in Table 3.

This effective gap size also accounts empirically for the heat transfer at the wall as a result of the very small direct contact area between wall and foam (end point of the struts touching the internal tube wall) and the effects due to the irregularity of the cylindrical foam shape, foam struts, different cell diameters, different methods of cutting the samples, and the presence of open cells. It appears that this effective gap size increases with increasing cell size. As shown in Fig. 7, the optimal estimates of the effective gap sizes for the 8 foams exhibit in fact a positive correlation with the cell diameter of the foam. The results from the heat transfer runs on all foams were used to find the following linear correlation (expressed in mm):

$$Eff. \, gap \, size = 0.13 + 0.14 \, d_c \tag{24}$$

It is noted that in applications with a significant physical gap between the inner surface of the reactor and the outer surface of the foam, this gap should be added to the effective gap size from this correlation.

This result is partially consistent with previous reports. In our earlier work [45], we proposed the following correlation to evaluate the wall heat transfer coefficient:

$$h_W = \frac{k_f}{d_C}(7.18 + 0.029 Re_{d_c}^{0.8}); 4 < Re_{d_c} < 255 \tag{25}$$

The static term closely resembles the findings of the present work only if the constant part of the in Eq. (26) is neglected. Such a discrepancy is possibly due to the larger cell size, d_c, of the previously investigated samples, which ranged from 1.55 mm to 5.09 mm, with respect to that of the foams herein investigated, which spans from 0.58 to 1.2 mm and could make more evident the effect of a radial physical gap between the tube and the boundary of the foam structure.

To take into account the convective contribution of the flowing gasses, an equation for the Nusselt number is proposed as follows [48,49]:

$$Nu = h_{Convection} d_c / k_f = C_1 Re_{d_c}^{0.8} Pr^{1/3} \tag{26}$$

where, Nu: Nusselt number [–]; $h_{Convection}$: the dispersive contribution of the fluid [W m^{-2} K^{-1}]; C_1: constant for dependency of the dynamic contribution to the heat transfer coefficient [–]; k_f: gas thermal conductivity [W m^{-1} K^{-1}]; Re_{dC}: Reynolds number based on cell diameter [–]; Pr: Prandtl number [–].

In this work, the global regression results forced the C_1 value to the zero-value constraint, which indicates that the convective contribution to the wall heat transfer is very small in comparison to the static one.

The radiative contribution is taken into account according to [48,49]:

$$h_{Radiation} = 4C_{1rad}\sigma T^3 \tag{27}$$

where, $h_{Radiation}$: contribution of radiation in the wall heat transfer coefficient [W m^{-2} K^{-1}]; C_{1rad}: radiation contribution factor [–]; σ: Stefan-Boltzman constant 5.67×10^{-8} [W m^{-2} K^{-4}]; T: temperature [K]. Optimization of this value resulted in constant slightly higher than 1 which is physically not possible. C_{1rad} was therefore fixed at the highest physically feasible value of 1.0.

5. Global fit: Results and discussion

5.1. Experimental temperature profiles and global fit results

As mentioned above, each experimental dataset from each run contains temperature measurements at 11 equidistant axial positions (every 5 mm, from the foam inlet until the end of the foam) and at the radial positions located at the centerline, 1/2 radius, and 2/3 radius and at the reactor wall. These experiments were performed at various conditions, with different foam materials, different cell diameters, and different conditions (flow type, temperature, and flow rate). The experimental results of the heat transfer
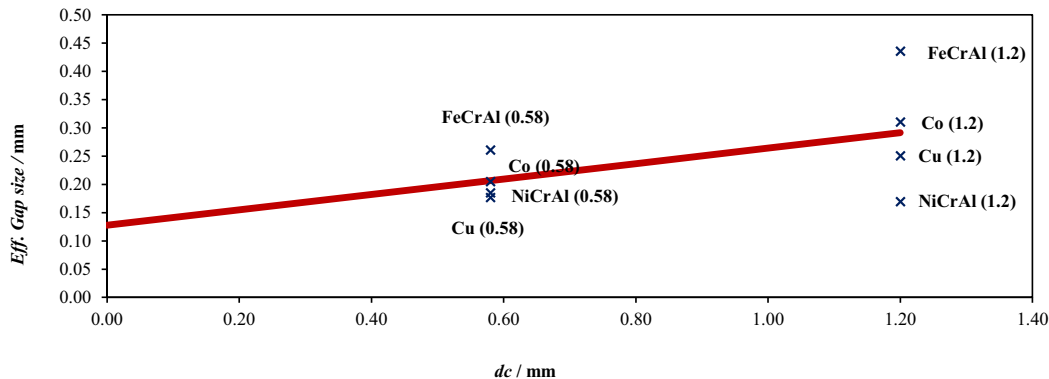
Fig. 7. The correlation between the effective gap size (Eff. gap size) and the foam cell diameter, d_c.

experiments are compared in Fig. 8 to the results of the optimal global fit obtained with the heat transfer model, described in Sections 3 and 4. Fig. 8 shows the optimal fit for the low-conductive NiCrAl alloy foam and the high-conductive Cu foam at temperatures 500 °C for N_2 and He at a flow rate of 30 Nl min^{-1}. The fit quality for the other experiments is well comparable. In all the figures the model describes the experimentally measured temperature well. The Athena built-in LSGREG solver was used to find the optimal parameters estimates by minimization of the SSQ of the differences between the experimental and the model data for all the experiments. For this, LSGREG solved the whole 2D model for all the experiments repeatedly while adapting and eventually optimizing the 20 parameters. The correlation matrix for the estimated parameters shows that there are no strong correlations between any of the parameters, confirming that the model contains no strongly correlated parameters and thus allowing accurate parameter estimation [59]. The correlation matrix and the parameter confidence ranges are explicitly described in Appendix B.

5.2. Estimated heat transfer coefficients and the effects of the operation conditions

In order to show the dependencies of the radial effective thermal conductivities and of the wall heat transfer coefficient according to the correlations, and to visualize the parameter estimation results, they are calculated at different conditions with results shown in Fig. 9 for the poorly conductive NiCrAl alloy foam and

for the highly conductive Cu foam, respectively. The highest effective radial conductivities are obtained for the copper foam with a k_{er} value of about 4.5 [W m^{-1} K^{-1}], which hardly depends on temperature and gas type. This is due to the largely dominant contribution of the solid thermal conductivity of the foam material to the total effective stagnant radial thermal conductivity, which widely overcomes contributions by conduction via the gas phase and radiation. Noteworthy the radial effective conductivity can be incremented several times by adopting conductive foams with higher fractions of solid material (as opposite to only 4% in foam G), as e.g. proposed in [67].

The properties of the flowing gas also largely determine the wall heat transfer coefficient, h_w. This indicates the dominant contribution of static conduction through the effective gap at the foam wall boundary. h_w also increases with the oven temperature mainly due to the positive effect of temperature on the fluid thermal conductivity and, to a lesser extent, to the enhanced contribution of radiation.

Noteworthy, thanks to the very high pore density of the investigated foams, estimates of the wall heat transfer coefficient higher than 1500 W m^{-2} K^{-1} have been obtained when using He as flowing gas, which is quite promising in view of the development and application of structured catalysts with enhanced heat transfer performances for process intensification. Notably, the thermal conductivity of He may be regarded as representative of the thermal conductivity of syngas (e.g. 0.244 W m^{-1} K^{-1} for He vs. 0.243 W m^{-1} K^{-1} for syngas with H_2/CO = 70/30 at 573 K [50]).

Foam D, NiCrAl alloy, d_c=1.2 mm, 500 °C, N_2, 30 Nl min^{-1}. Foam D, NiCrAl alloy, d_c=1.2 mm, 500 °C, He, 30 Nl min^{-1}.

Foam H, Copper, d_c=1.2 mm, 500 °C, N_2, 30 Nl min^{-1}. Foam H, Copper, d_c=1.2 mm, 500 °C, He, 30 Nl min^{-1}.
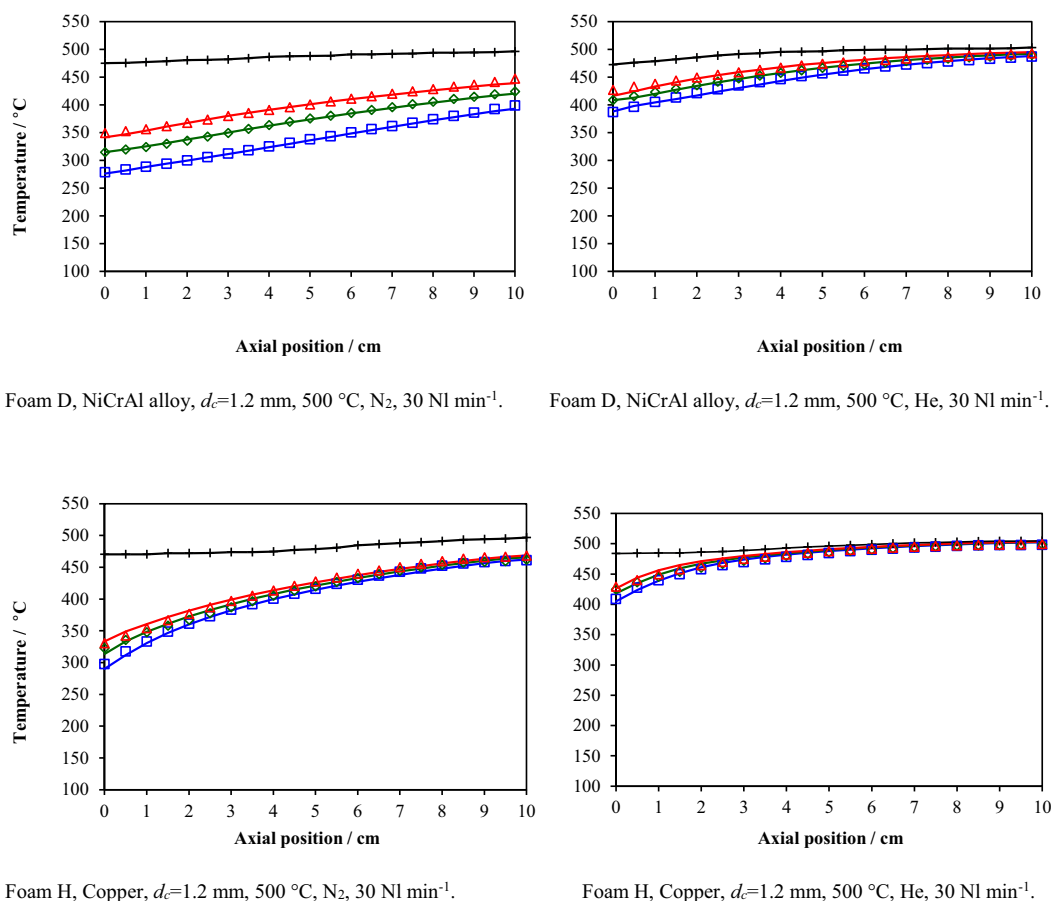
Fig. 8. Four typical axial temperature profiles for the used foam samples (the symbols are the experimental data and the curves correspond to the optimal fit with the general model). The following abbreviations and legend apply experimental temperature measurement at center, 1/2, 2/3 radius and reactor tube wall, Exp(0) □, Exp(1/2) ◇, Exp(2/3) △, and Wall +. Simulation results (optimal fit) at center, 1/2, 2/3 radius, Sim(0) ▬, Sim(1/2) ▬, and Sim(2/3) ▬.
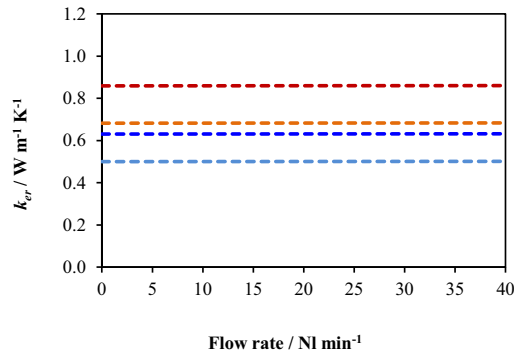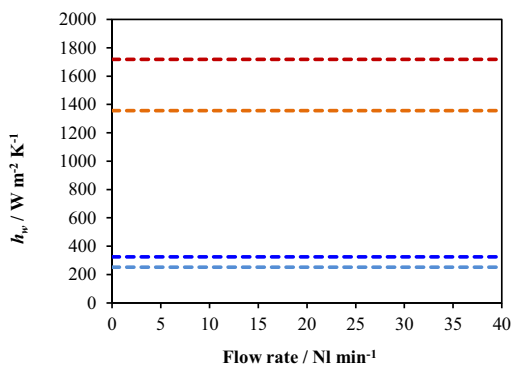
Foam C, NiCrAl alloy, d_c=0.58 mm, k_{er} vs. flow rate
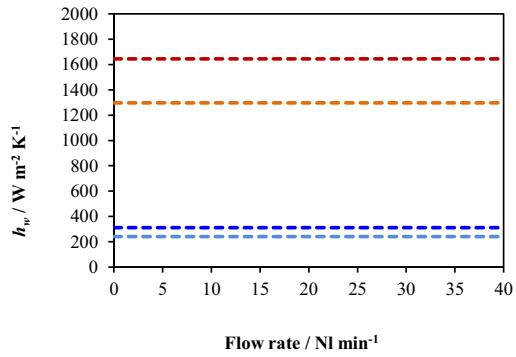
Foam C, NiCrAl alloy, d_c=0.58 mm, h_w vs. flow rate
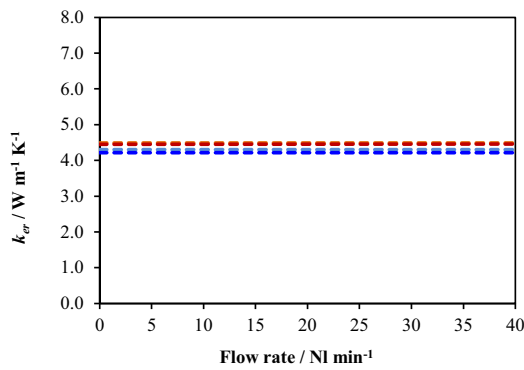
Foam G, copper, d_c=0.58 mm, k_{er} vs. flow rate

Foam G, copper, d_c=0.58 mm, h_w vs. flow rate

Fig. 9. The radial effective conductivity and wall heat transfer coefficient plotted versus flow rate. The following abbreviations and legend are used: global regression results (optimal fit): N_2 at 300 °C ━ ━, N_2 at 500 °C ━ ━, He at 300 °C ━ ━, He at 500 °C ━ ━.

6. Conclusions

The open-cell metal foams with very high cell densities used in this study show a promising future as catalyst supports due to their high radial effective thermal conductivities (up to 4.5 W m^{-1} K^{-1} for copper foams), which hold potential to improve the heat management in non-adiabatic tubular reactors for exothermic chemical processes, resulting in increased productivities and selectivities. Based on experimental heat transfer data obtained over a large number of different metal foams with various materials, geometrical properties, and porosities, at various temperatures, gas types, and gas flow rates, a general correlation was developed successfully for estimation of the effective thermal conductivity and the wall heat transfer coefficient. This correlation can be used to predict the thermal behavior of foams of different materials over a wide range of conditions in different applications. Examples are tubular reactors for strongly exothermic or endothermic catalytic reactions, such as e.g. partial oxidation of methanol to formaldehyde or methane steam reforming. In line with previous findings, the present results over foams with high cell densities show that the conductive contribution dominates the radial effective thermal conductivity, and the often used Lemlich constant can be a reliable engineering guess for the conductive efficiency (the A parameter in this study), whereas the heat transport resistance in the gas between the inner surface of the reactor tube and outer surface of the foam provides the main contribution to the wall heat transfer coefficient. This contribution is directly proportional to the thermal conductivity of the flowing gas and inversely proportional to an "effective gap size" increasing with cell diameter. This indicates that in the structured tubular reactor the wall heat transfer

coefficient (h_w) is essentially independent of the flow rate. Therefore, there is no need any more for very high flow velocities to achieve high heat transfer rates, as requested instead in conventional packed-bed reactors. Hence, this enables tubular reactor designs with shorter tubes, thus resulting in compact configurations (process intensification) and in smaller pressure drop (reduction in energy costs). Moreover, structured reactors which can operate at partial loadings without diminishing the heat transfer efficiency would significantly increase the flexibility of the system [68–70].

Appendix A

The inlet zone of the foam sample is defined as the volume between 5 mm before the foam and the foam itself. Similarly to previous reports [47], a FeCrAl alloy foam was placed in the upstream zone contacting the foam bed (foam sample) to improve the uniformity of inlet gas flow and temperature profile over the radius.

$$\begin{cases} k_{ea}\frac{\partial T}{\partial x} = W_{in}C_p\left(T_{x=0,r} - T_{x=-5mm,r}\right), & at : x = 0 \\ \frac{\partial T}{\partial x} = 0, & at : x = L \end{cases} \quad (A1)$$

The radial inlet temperature ($x = -5$ mm) profiles are described using the following equation, in which the values of $T(r = 0)$, a and b are different for each foam sample and conditions:

$$T = T(r = 0) + a\left(\frac{r}{R}\right)^b \quad (A2)$$

where, T: the local temperature [K]; $T(r = 0)$: temperature at $r = 0$ radial coordinate and $x = -5$ mm axial coordinate [K]; a and b: fitting parameters [–]; r: radial position [–]; R: foam external radius [–].

The radial inlet temperature profile thus contains three unknowns, $T(r = 0)$, a and b, whereas there are four conditions available at the axial coordinate of $x = -5$ mm and at the different radial positions: (i) T_0 at $r = 0$ (center), (ii) $T_{1/2}$ at r = 1/2 R, (iii) $T_{2/3}$ at r = 2/3 R, and the wall temperature (T_w) measuring the temperature of the outer surface of the reactor tube. Since the locations 1/2 R and 2/3 R are very close to each other, it was decided to take the average temperature of these two points in order to end up with three equations with three unknowns to fit the inlet radial temperature profiles in each experiment. Therefore, temperature at the axial coordinate x = -5 mm and radial coordinate of $r = (1/2 R + 2/3 R)/2$, is taken as:

$$T_p = \frac{T_{1/2} + T_{2/3}}{2} \quad (A3)$$

The temperature T_1 is assumed for the position of $x = -5$ mm and $r = R$. In other words, the temperature of the foam external surface at the inlet ($x = -5$ mm) is assumed to be T_1.

Therefore, at $r = (1/2R + 2/3 R)/2$, according to Eq. (A2):

$$T_p = T(r = 0) + a\left(0.25 + \frac{1}{3}\right)^b \quad (A4)$$

Also, at the outer surface of the foam, $r = R$, Eq. (A5) applies:

$$T_w - T_1 = \frac{k_{er}}{h_w}\frac{\partial T}{\partial r}\bigg|_{r=R} \quad (A5)$$

Considering Eq. (A2), the T derivative at r = R is:

$$\frac{k_{er}}{h_w}\frac{\partial T}{\partial r}\bigg|_{r=R} = \frac{k_{er}}{h_w}\left(\frac{ab}{R}\left(\frac{r}{R}\right)^{b-1}\right)_{r=R} = \frac{ab}{R}\frac{k_{er}}{h_w} \quad (A6)$$

And the temperature at the outer surface of the foam (T_1) is

$$T_1 = T(r = 0) + a\left(\frac{r}{R}\right)^b\bigg|_{r=R} = T(r = 0) + a \quad (A7)$$

Combining the two equations above finally yields:

$$T_w = T(r = 0) + a\left(1 + b\frac{k_{er}}{Rh_w}\right) \quad (A8)$$

The term k_{er}/Rh_w in the inlet zone might be estimated by e.g. literature correlations for k_{er} and h_w and using the actual value of R, but this yielded poor fits, probably as a result of the non-uniform velocity profile in the inlet zone. Therefore, it was decided to add the term k_{er}/Rh_w to the set of parameters to be optimized for the general fit. For obtaining good fits in the entrance part of the foams, it appeared necessary to fit two different values of this parameter for the two flowing gasses used in the experiments, N_2 and He. The parameter k_{er}/Rh_w corresponds to the inverse of the Biot number at the wall, which expresses the ratio of the heat transfer resistance inside a body and that at the external surface of a body, and therefore it is named "1/*Biot*". This parameter was thus optimized together with all other model parameters based on the best fit of the temperature profiles in the whole foam. It is stressed that this parameter "1/*Biot*" includes the effect of the non-uniform radial velocity profile, which may even contain a flow in backward direction at the wall, and that it, therefore, does not need to be a reasonable estimate of the ratio of k_{er}/R and h_w of the FeCrAl alloy foam positioned in the upstream zone. In this investigation, the radial velocity profile is probably quite non-uniform and different in the experiments conducted with N_2 and He.

This finally yields three equations with three unknowns, namely $T(r = 0)$, a, and b, which are solved by the Athena solver [62]:

$$\begin{aligned} T(r = 0) &= T_{r=0} \\ T_p &= T(r = 0) + a\left(0.25 + \tfrac{1}{3}\right)^b \\ T_w &= T(r = 0) + a\left(1 + b\tfrac{1}{Biot}\right) \end{aligned} \quad (A9)$$

As mentioned above, two different values of 1/*Biot* were optimized for the two different flowing gasses in our tests. These were constrained by a lower bound of 1E-6 to avoid crashing of the simulation model and negative values for the Biot number and an upper bound of 2.0, since it appears that this prevents b values below 1.0, which correspond to unrealistic concave radial temperature profiles (decreasing slope when getting closer to the wall) in the inlet zone instead of convex profiles (increasing slope when getting closer to the wall). The fit results returned different 1/*Biot* estimates for N_2 and He. In the experiments with He gas flow, quite some 1/*Biot* values are optimized at the lower bound of 1.0E-6, which might be related to the lower sensitivity of the inlet temperature profile to the foam temperature profiles with this highly conductive gas.

Appendix B

The correlation matrix for the estimated parameters, available in Table B1, shows that there are generally only limited correlations between the parameters, with the exception of the correlations between the A values and the Effective gap sizes of the same foams, up to a value of 0.84, which is however still acceptable. Indeed, all the parameters could be estimated with a confidence range smaller than the parameter absolute value.

Although the model we use in this work is non-linear, it is in most cases still accurate to assume that the 95% confidence range of a parameter is inversely proportional to the square root of the total number of degrees of freedom, provided that the experimental error has zero mean and constant, independently distributed variance [71]. According to Froment et al. [71], the total number of degrees of freedom is the number of experimental data points minus the total number of optimized parameters:

$$\begin{aligned} \text{Degrees of freedom}_{\text{Total}} =\ & N_{\text{Experimental data points}} \\ & - N_{\text{optimized parameters}} \end{aligned} \quad (B1)$$

Due to the high thermal conductivity of the foams it seems, however, not accurate to assume that the 63 experimental data points for each heat transfer run are completely independent. In order to correct for the correlation between the 63 experimental data points in one experiment, the number of independent data points is assumed to be one order of magnitude smaller, i.e. a factor 10 smaller (resulting in 6.3 independent data points per experiment). Then, the confidence ranges from the parameter estimation were modified for this accordingly (taking into account that 20 parameters have been estimated):

$$\frac{95\% \text{ confidence range (modified)}}{95\% \text{ confidence ranges (model)}} = \frac{\sqrt{8 \times 8 \times 63 - 20}}{\sqrt{8 \times 8 \times 6.3 - 20}} = 3.24$$

$$(B2)$$

Table B1

Correlation matrix between all the parameters estimated with the simulation model.

|	A (foam A)	A (foam B)	A (foam C)	A (foam D)	A (foam E)	A (foam F)	A (foam G)	A (foam H)	Eff. gap size (foam A)	Eff. gap size (foam B)	Eff. gap size (foam C)	Eff. gap size (foam D)	Eff. gap size (foam E)	Eff. gap size (foam F)	Eff. gap size (foam G)	Eff. gap size (foam H)	$C_{Ross.}$	$1/$ Biot N_2	$1/$ Biot He
A (foam A)	1																		
A (foam B)	0.15	1																	
A (foam C)	0.05	0.12	1																
A (foam D)	0.14	0.33	0.11	1															
A (foam E)	0.07	0.16	0.06	0.16	1														
A (foam F)	0.16	0.36	0.13	0.35	0.18	1													
A(foam G)	0.02	0.04	0.02	0.04	0.03	0.06	1												
A (foam H)	0.05	0.09	0.04	0.08	0.06	0.11	0.04	1											
Eff. gap size (foam A)	0.79	−0.04	−0.02	−0.03	−0.03	−0.05	−0.03	−0.04	1										
Eff. gap size (foam B)	−0.05	0.54	−0.04	−0.09	−0.05	−0.11	−0.04	−0.06	0.03	1									
Eff. gap size (foam C)	−0.01	−0.03	0.84	−0.02	−0.02	−0.03	−0.02	−0.03	0.02	0.02	1								
Eff. gap size (foam D)	−0.03	−0.07	−0.03	0.63	−0.04	−0.08	−0.03	−0.04	0.02	0.04	0.02	1							
Eff. gap size (foam E)	−0.01	−0.01	−0.01	0.00	0.83	−0.01	−0.02	−0.02	0.02	0.02	0.01	0.01	1						
Eff. gap size (foam F)	−0.04	−0.07	−0.03	−0.07	−0.04	0.57	−0.03	−0.04	0.02	0.04	0.02	0.03	0.01	1					
Eff. gap size (foam G)	−0.01	−0.01	0.00	−0.01	−0.01	−0.01	0.78	−0.01	0.01	0.01	0.01	0.01	0.01	0.01	1				
Eff. gap size (foam H)	−0.01	−0.01	−0.01	−0.01	−0.01	−0.01	−0.01	0.79	0.01	0.01	0.01	0.01	0.01	0.01	0.00	1			
$C_{Ross.}$	0.25	0.57	0.20	0.57	0.28	0.61	0.06	0.14	−0.05	−0.14	−0.03	−0.11	0.00	−0.11	−0.01	−0.01	1		
$1/$Biot N_2	0.11	0.20	0.09	0.15	0.14	0.26	0.17	0.24	−0.15	−0.20	−0.11	−0.15	−0.10	−0.14	−0.05	−0.07	0.00	1	
$1/$Biot He	−0.02	0.01	−0.02	0.01	−0.01	0.01	−0.01	0.02	−0.02	−0.02	−0.02	−0.02	−0.01	−0.02	−0.01	0.01	0.04	0.00	1
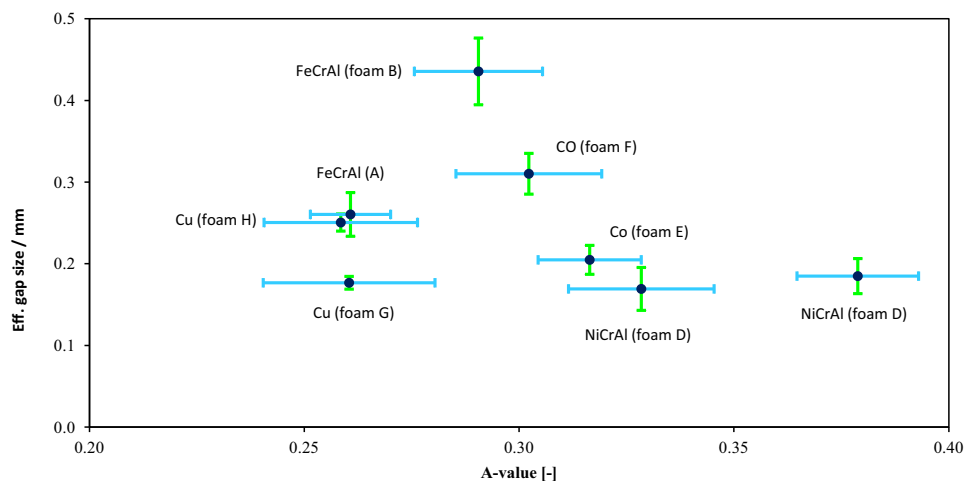
Fig. B1. Illustration of Eff. gap sizes vs. values of A with the error bars increased by a factor 3.24, based on the assumption that the number of independent data points is approximately a factor 10 smaller than the total number of experimental data points.

It should be noted that the experimental points for 8 foams, done at 8 different experimental conditions, and 21 points axial and 3 points radial are equal to 63. Fig. B1 shows the estimated 8 Eff. gap sizes versus the 8 optimized A parameters. The 95% confidence ranges from Table 3 in this paper, multiplied with the factor of 3.24, are indicated.

Fig. B1 shows that also after this correction the confidence ranges do not overlap one specific Eff. gap size or A. In other words, there is clearly not one specific A or Eff. gap size that falls within the confidence ranges of all the 8 tested foam samples. This proves the need for optimizing both parameters for each foam separately, including the effects of structure and material properties. Moreover, the graph seems to show a cloud of points rather than a clear correlation, although one might see a negative correlation between both parameters. Such a negative correlation, however, contradicts the positive correlation obtained between Eff. gap size and A parameter in the correlation matrix from the parameter estimation model. Therefore, the slightly negative correlation between the A and Eff. Gap size seems to be not systematic but just a coincidence and/or related with the individual foam characteristics, i.e. differences in foam structure and precision of the cylindrical shape of the foam.

References

[1] P. Chin, X. Sun, G.W. Roberts, J.J. Spivey, Preferential oxidation of carbon monoxide with iron-promoted platinum catalysts supported on metal foams, Appl. Catal. A 302 (2006) 22–31.

[2] A. Sirijaruphan, J.G. Goodwin Jr., R.W. Rice, D. Wei, K.R. Butcher, G.W. Roberts, J.J. Spivey, Effect of metal foam supports on the selective oxidation of CO on Fe-promoted Pt/ γ-Al₂O₃, Appl. Catal. A 281 (2005) 11–18.

[3] F. Scheffler, R. Herrmann, W. Schwieger, M. Scheffler, Preparation and properties of an electrically heatable aluminum foam/zeolite composite, Microporous Mesoporous Mater. 67 (2004) 53–59.

[4] F. Bidault, D.J.L. Brett, P.H. Middleton, N. Abson, N.P. Brandon, A new application for nickel foam in alkaline fuel cells, Int. J. Hydrogen Energy 34 (2009) 6799–6808.

[5] E.J. Cookson, D.E. Floyd, A.J. Shih, Design and analysis of metal foam electrical resistance heater, Int. J. Mech. Sci. 48 (2006) 1314–1322.

[6] L. Giani, G. Groppi, E. Tronconi, Mass-transfer characterization of metallic foams as supports for structured catalysts, Ind. Eng. Chem. Res. 44 (14) (2005) 4993–5002.

[7] Y. Peng, J.T. Richardson, Properties of ceramic foam catalyst supports: one-dimensional and two-dimensional heat transfer correlations, Appl. Catal. A 266 (2004) 235–244.

[8] M.F. Ashby, Metal Foams: A Design Guide, Elsevier, 2000.

[9] N. Dukhan, Metal Foams: Fundamentals and Applications, DEStech Publications Inc., 2013.

[10] L.J. Gibson, M.F. Ashby, Cellular Solids: Structure and Properties, Pergamon Press, Oxford, U.K., 1988.

[11] L.J. Gibson, M.F. Ashby, Cellular Solids: Structure and Properties, second ed., University of Cambridge Press, Cambridge, U.K., 1999.

[12] C. Hutter, A. Zenklusen, R. Lang, Ph. Rudolf von Rohr, Axial dispersion in metal foams and streamwise-periodic porous media, Chem. Eng. Sci. 66 (2011) 1132–1141.

[13] F.C. Buciuman, B. Kraushaar-Czarnetzki, Ceramic foam monoliths as catalyst carriers. 1. Adjustment and description of morphology, Ind. Eng. Chem. Res. 42 (2003) 1863–1869.

[14] M.V. Twigg, J.T. Richardson, Fundamentals and application of structured ceramic foam catalysts, Ind. Eng. Chem. Res. 46 (2007) 4166–4177.

[15] J.T. Richardson, Y. Peng, D. Remue, Properties of ceramic foam catalyst supports: pressure drop, Appl. Catal. A 204 (2000) 19–32.

[16] M. Sheng, H. Yang, D.R. Cahela, B.J. Tatarchuk, Novel catalyst structures with enhanced heat transfer characteristics, J. Catal. 281 (2011) 254–262.

[17] M.V. Twigg, J.T. Richardson, Theory and applications of ceramic foam catalysts, Chem. Eng. Res. Des. 80 (2002) 183–189.

[18] D.A. Hickman, L.D. Schmidt, Synthesis gas formation by direct oxidation of methane over Pt monoliths, J. Catal. 138 (1992) 267–282.

[19] D.A. Hickman, L.D. Schmidt, Production of syngas by direct catalytic oxidation of methane, Science 259 (1993) 343–346.

[20] D.A. Hickman, E.A. Haupfear, L.D. Schmidt, Synthesis gas formation by direct oxidation of methane over Rh monoliths, Catal. Lett. 17 (1993) 223–237.

[21] M. Huff, P.M. Torniainen, D.A. Hickman, L.D. Schmidt, Partial Oxidation of CH₄, C₂H₆, and C₃H₈ on Monoliths at Short Contact Times, In Studies in Surface Science and Catalysis 81, Curry-Hyde, Elsevier, Amsterdam, 1994.

[22] M. Huff, L.D. Schmidt, Oxidative dehydrogenation of isobutane over monoliths at short contact times, J. Catal. 155 (1995) 82–94.

[23] A.G. Dietz, A.F. Carlsson, L.D. Schmidt, Partial oxidation of C5 and C6 Alkanes over monolith catalysts at short contact times, J. Catal. 176 (1996) 459–473.

[24] E.C. Wanat, B. Suman, L.D. Schmidt, Partial oxidation of alcohols to produce hydrogen and chemicals in millisecond reactors, J. Catal. 235 (2005) 18–27.

[25] K.A. Williams, L.D. Schmidt, Catalytic autoignition of higher alkane partial oxidation on Rh-coated foams, Appl. Catal. A 299 (2006) 30–45.

[26] R. Subramanian, L.D. Schmidt, Renewable olefins from biodiesel by autothermal reforming, Angew. Chem. Int. Ed. 44 (2005) 302–305.

[27] V.V. Calmidi, R.L. Mahajan, The effective thermal conductivity of high porosity fibrous metal foams, J. Heat Transfer 121 (2) (1999) 466–471.

[28] M.F. Ashby, A.G. Evans, N.A. Fleck, L.J. Gibson, J.W. Hutchinson, H.N.G. Wadley, Metal Foams: A Design Guide, Butterworth Heinemann, Oxford, 2000.

[29] J.C. Maxwell, A Treatise on Electricity and Magnetism, vol. 1, Clarendon Press, 1873.

[30] R. Lemlich, A theory for the limiting conductivity of polyhedral foam at low density, J. Colloid Interface Sci. 64 (1) (1978) 107–110.

[31] S. Langlois, F. Coeuret, Flow-through and flow-by porous electrodes of nickel foam. I. Material characterization, J. Appl. Electrochem. 19 (1) (1989) 43–50.

[32] B. Ozmat, B. Leyda, B. Benson, Thermal applications of open-cell metal foams, Mater. Manuf. Processes 19 (5) (2004) 839–862.

[33] E.N. Schmierer, A. Razani, Self-consistent open-celled metal foam model for thermal applications, J. Heat Transfer 128 (2006) 1194–1203.

[34] B. Dietrich, G. Schell, E.C. Bucharsky, R. Oberacker, M.J. Hoffmann, W. Schabel, M. Kind, H. Martin, Determination of the thermal properties of ceramic sponges, Int. J. Heat Mass Transfer 53 (1–3) (2009) 198–205.

[35] A. Bhattacharya, V.V. Calmidi, R.L. Mahajan, Thermophysical properties of high porosity metal foams, Int. J. Heat Mass Transfer 45 (5) (2002) 1017–1031.

[36] G.N. Dul'nev, Heat transfer through solid disperse systems, J. Eng. Phys. 9 (3) (1965) 399–404.

[37] J.G. Fourie, J.P. Du Plessis, Effective and coupled thermal conductivities of isotropic open-cellular foams, AIChE J. 50 (3) (2004) 547–556.

[38] K. Boomsma, D. Poulikakos, On the effective thermal conductivity of a three dimensionally structured fluid-saturated metal foam, Int. J. Heat Mass Transfer 44 (4) (2001) 827–836.

[39] K. Boomsma, D. Poulikakos, Corrigendum for the paper: K. Boomsma, D. Poulikakos", On the effective thermal conductivity of a three-dimensionally structured fluid-saturated metal foam"[International Journal of Heat and Mass Transfer 44 (2001) 827–836], Int. J. Heat Mass Transfer 54 (1) (2011) 746–748.

[40] Z. Dai, K. Nawaz, Y.G. Park, J. Bock, A.M. Jacobi, Correcting and extending the Boomsma-Poulikakos effective thermal conductivity model for three dimensional, fluid-saturated metal foams, Int. Commun. Heat Mass Transfer 37 (6) (2010) 575–580.

[41] D. Edouard, The effective thermal conductivity for "Slim" and "Fat" foams, AIChE J. 57 (6) (2010) 1646–1651.

[42] S. Krishnan, S.V. Garimella, J.Y. Murthy, Simulation of thermal transport in open-cell metal foams: effect of periodic unit-cell structure, J. Heat Transfer 130 (2008), 024503/1-5.

[43] R. Singh, H.S. Kasana, Computational aspects of effective thermal conductivity of highly porous metal foams, Appl. Therm. Eng. 24 (13) (2004) 1841–1849.

[44] E. Bianchi, T. Heidig, C.G. Visconti, G. Groppi, H. Freund, E. Tronconi, An appraisal of the heat transfer properties of metallic open-cell foams for strongly exo-/endo-thermic catalytic processes in tubular reactors, Chem. Eng. J. 198–199 (2012) 512–528.

[45] E. Bianchi, T. Heidig, C.G. Visconti, G. Groppi, H. Freunda, E. Tronconi, Heat transfer properties of metal foam supports for structured catalysts: wall heat transfer coefficient, Catal. Today 216 (2013) 121–134.

[46] http://www.alantum.com/.

[47] C.Y. Zhao, T.J. Lu, H.P. Hodson, J.D. Jackson, The temperature dependency of effective thermal conductivity of open-celled steel alloy foams, Mater. Sci. Eng., A 367 (1–2) (2004) 123–131.

[48] J.P. Holman, Heat Transfer, McGraw-Hill, New York, 1989.

[49] A. Bejan, A.D. Kraus, Heat Transfer Handbook, John Wiley & Sons, Inc., New Jersey, 2003.

[50] R.H. Perry, W.G. Green, Perry's Chemical Engineers' Handbook, McGraw-Hill, New York, 2008.

[51] C.Y. Zhao, T.J. Lu, H.P. Hodson, Thermal radiation in ultralight metal foams with open cells, Int. J. Heat Mass Transfer 47 (14–16) (2004) 2927–2939.

[52] G.I. Garrido, F.C. Patcas, S. Lang, B. Kraushaar-Czarnetzki, Mass transfer and pressure drop in ceramic foams: a description for different pore sizes and porosities, Chem. Eng. Sci. 63 (21) (2008) 5202–5217.

[53] R. Coquard, M. Loretz, D. Baillis, Conductive heat transfer in metallic/ceramic open-cell foams, Adv. Eng. Mater. 10 (4) (2008) 323–337.

[54] E. Bianchi, W. Schwieger, H. Freund, Assessment of periodic open cellular structures for enhanced heat conduction in catalytic fixed-bed reactors, Adv. Eng. Mater. 18 (4) (2016) 608–614.

[55] A. Inayat, H. Freund, T. Zeiser, W. Schwieger, Determining the specific surface area of ceramic foams: the tetrakaidecahedra model revisited, Chem. Eng. Sci. 66 (2011) 1179–1188.

[56] P.V. Danckwerts, Continuous flow systems: distribution of residence times, Chem. Eng. Sci. 2 (1953) 1–13.

[57] I. Langmuir, The velocity of reactions in gases moving through heated vessels and the effect of convection and diffusion, J. Am. Chem. Soc. 30 (11) (1908) 1742–1754.

[58] J.F. Liu, W.T. Wu, W.C. Chiu, W.H. Hsieh, Measurement and correlation of friction characteristic of flow through foam matrixes, Exp. Therm. Fluid Sci. 30 (4) (2006) 329–336.

[59] Athena Visual Studio, Software for modeling, estimation and optimization, Version 12.1, www.AthenaVisual.com.

[60] M. Wallenstein, M. Kind, B. Dietrich, Radial two-phase thermal conductivity and wall heat transfer coefficient of ceramic sponges – experimental results and correlation, Int. J. Heat Mass Transfer 79 (2014) 486–495.

[61] M.L. Hunt, C.L. Tien, Effects of thermal dispersion on forced convection in fibrous media, Int. J. Heat Mass Transfer 31 (2) (1988) 301–309.

[62] P.-F. Hsu, J.R. Howell, Measurements of thermal conductivity and optical properties of porous partially stabilized zirconia, Exp. Heat Transfer 5 (4) (1992) 293–313.

[63] C.Y. Zhao, S.A. Tassou, T.J. Lu, Analytical considerations of thermal radiation in cellular metal foams with open cells, Int. J. Heat Mass Transfer 51 (3–4) (2008) 929–940.

[64] V.V. Calmidi, R.L. Mahajan, Forced convection in high porosity metal foams, J. Heat Transfer 122 (3) (2000), 557foam.

[65] L. Glicksman, M. Schuetz, M. Sinofsky, Radiation heat transfer in foam insulation, Int. J. Heat Mass Transfer 30 (1) (1987) 187–197.

[66] M. Loretz, E. Maire, D. Baillis, Analytical modeling of the radiative properties of metallic foams: contribution of X-ray tomography, Adv. Eng. Mater. 10 (4) (2008) 352–360.

[67] A. Montebelli et al., Optimization of compact multitubular fixed-bed reactors for the methanol synthesis loaded with highly conductive structured catalysts, Chem. Eng. J. 255 (2014) 257–265.

[68] Patent applications WO/2010/130399 and WO/2014/102350 (packed monolith).

[69] Patent application WO/2015/033266 (packed foams).

[70] C.G. Visconti, G. Groppi, E. Tronconi, Highly conductive "packed foams": a new concept for the intensification of strongly endo- and exo-thermic catalytic processes in compact tubular reactors, Catal. Today 273 (2016) 178–186.

[71] G.F. Froment, K.B. Bischoff, Chemical Reactor Analysis and Design, John Wiley & Sons, New York, 1990.